Theory of High-Harmonic Gyrotron Oscillators with Slotted Cross-Section Structure

P. VITELLO AND C. MENYUK

Abstract—**A linear-theory analysis of gyrotron oscillators with slotted cross section is used to calculate the net change in beam energy $\langle \delta\gamma \rangle_{l,o\varphi_o}$. In our new formalism, geometric factors are clearly distinguished from the geometry-independent harmonic resonance terms which are due to the fundamental electron cyclotron maser and peniotron interactions. This separation of the interaction terms from the geometric factors greatly simplifies the physical analysis, and leads to a very compact form for $\langle \delta\gamma \rangle_{l,o\varphi_o}$. The theory is applied to slotted rectangular oscillators (which have not previously been treated) and to slotted cylindrical oscillators to show that a unified expression can be obtained for the start oscillation condition. In sample applications of our theory, it is demonstrated that slots lower the start oscillation condition in both cylindrical and rectangular geometries, and can lead to a *decrease* in this condition as harmonic number is increased in the rectangular geometry. The use of these slotted devices thus appears quite attractive in the millimeter-wave regime. We also find that the peniotron interaction, which is easily identified in our formalism, may be very strong in slotted cavities.**

I. INTRODUCTION

THE GYROTRON is well known as a coherent microwave source capable of generating unprecedented power levels. Gyrotron emission occurs at harmonics of the electron cyclotron frequency. As the emission frequency increases, either large magnetic fields must be used or operation at high-cyclotron harmonics is required. Currently, most gyrotron development has focused on devices using either the first or second harmonics [1]–[3]. These low harmonics necessitate the use of a superconducting magnet if frequencies as high as the millimeter and submillimeter wave regimes are to be achieved.

High-harmonic gyrotron emission has been achieved for several tube designs. Using smooth-walled cylindrical cavities and an axis-encircling beam, harmonics as high as $m = 11$ have been observed for a TE_{m1l} "whispering gallery" mode gyrotron oscillator [4], [5]. A high-energy, large-Larmor-orbit beam is required for "whispering gallery" mode gyrotrons as these modes tend to concentrate the RF field towards the wall of the cavity. Also using an axis-encircling beam with high-energy (2 MeV) electrons, Destler *et al.* [6] have reported the generation of a strong burst of microwave radiation at the 12th harmonic from a slotted cylindrical tube. This new interactive slotted structure leads to an excellent high-harmonic interaction and good mode selection. Further investigations of slotted cylindrical tubes [7]–[15] and of slotted rectangular and ridged rectangular tubes [16]–[19] have shown that even for moderate beam energies, strong high-harmonic fringe fields can be positioned at the beam orbits. Two slotted tube geometries, shown in Fig. 1, have been investigated in detail; these are the cylindrical (or magnetron-type) geometry, and rectangular geometries, both slotted and ridged. As there is no real distinction between slotted and ridged tubes, we will refer to them all as slotted. Both gyro-TWT amplifiers [7]–[10] and gyrotron oscillators [11]–[15] have been studied theoretically in slotted cylindrical geometries. For rectangular geometries only, gyro-TWT amplifiers have been studied in detail for slotted cavities [16]–[19]. All of these studies show that slotted structures greatly increase the high-harmonic interaction in a gyrotron relative to a smooth wall design.

In this paper we extend the modeling of slotted gyrotron oscillators by presenting a linear kinetic theory applicable to gyrotrons of both rectangular and cylindrical cross-section design. In our analysis we calculate the net energy loss of the beam $\langle \delta\gamma \rangle_{l,o\varphi_o}$ which is needed to determine the cavity start oscillation condition and the frequency detuning. We give $\langle \delta\gamma \rangle_{l,o\varphi_o}$ as a sum over harmonics in which each harmonic contribution consists of a geometry-independent factor due to the fundamental interactions and a geometry-dependent factor, which varies from device to device. The geometry-independent factor consists of clearly distinguished terms due to the electron cyclotron maser and peniotron interactions.

This paper is organized as follows. In Section II, we derive the TE mode fields in either rectangular or cylindrical slotted cavities. Two specific examples are presented which are then used in the remainder of the paper. In Section III, we present our linear theory and determine the start oscillation condition and frequency detuning of the oscillator cavity modes. In Section IV, we present sample calculations which show both the strong high-harmonic content of slotted cavities, and the importance of peniotron emission for these systems.

Manuscript received July 29, 1987; revised December 4, 1987. This work was supported by the Air Force Office of Scientific Research under Contract F49620-86-C-065, and by the University of California at Los Angeles under Contract 400093 through the U.S. Army Research Office Contract ARO-DAAG 29-92-K-0004.

P. Vitello is with Science Applications International Corporation, McLean, VA 22102.

C. Menyuk is with the Department of Electrical Engineering, University of Maryland, Catonsville, MD 21228, and College Park, MD 20742.

IEEE Log Number 8819786.

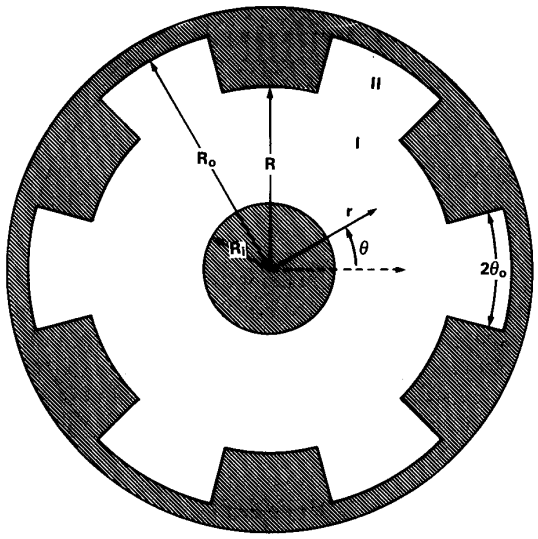

(a)

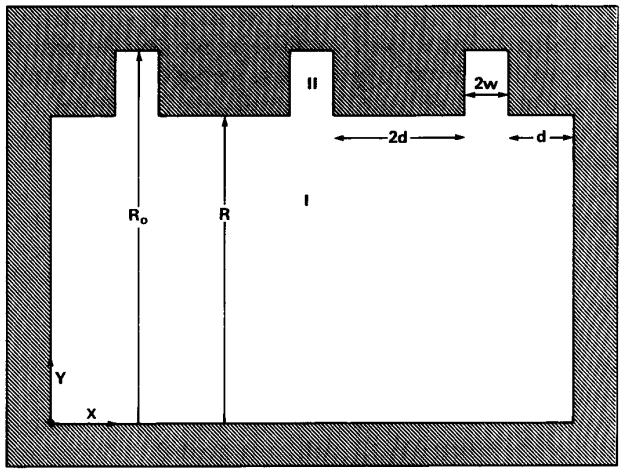

(b)

Fig. 1. (a) Cross section of the slotted cylindrical gyrotron. (b) Cross section of the slotted rectangular gyrotron.

II. Properties of Slotted Cavity Fields

Let us consider the behavior of the TE modes in a tube with a slotted cross section. If the axial RF magnetic field is written in the form

$$B_z = A_T(x, y) f(z) e^{-i\omega t} \tag{1}$$

(where $f(z) = e^{ik_z z}$ for an amplifier and $f(z) = \sin(k_z z)$ for an oscillator), then from Maxwell's equations [20] the solution for A_T will be an eigenfunction of the equation

$$(\vec{\nabla}_T \cdot \vec{\nabla}_T + k_\perp^2) A_T = 0 \tag{2}$$

subject to the boundary conditions of an assumed perfectly conducting tube wall. In (2), $k_\perp^2 = \omega^2 - k_z^2$ is the transverse wavenumber eigenvalue, and $\vec{\nabla}_T$ is the transverse Laplacian. The transverse RF electric and magnetic fields, $\vec{E}_T$ and $\vec{B}_T$, may be obtained from B_z as follows:

$$\vec{E}_T = -i \frac{\omega}{k_\perp^2} (\hat{z} \times \vec{\nabla}_T B_z) \tag{3}$$

$$\vec{B}_T = \frac{1}{k_\perp^2} \frac{\partial}{\partial z} \vec{\nabla}_T B_z. \tag{4}$$

Two sets of orthogonal eigenfunction basis sets are commonly used to describe A_T in slotted cavities. If the cross section is naturally specified in a Cartesian coordinate system, then the solution

$$A_T(x, y) = \sum_{\Gamma=-\infty}^{\infty} \mathcal{C}_\Gamma (e^{-ik_{x\Gamma}x} + a_\Gamma e^{ik_{x\Gamma}x}) \cdot (e^{-ik_{y\Gamma}y} + b_\Gamma e^{ik_{y\Gamma}y}) \tag{5}$$

where $k_{x\Gamma}^2 + k_{y\Gamma}^2 = k_\perp^2$, should be used. For a cross section with cylindrical symmetry,

$$A_T(r, \theta) = \sum_{\Gamma=-\infty}^{\infty} \mathcal{C}_\Gamma \mathcal{C}_\Gamma(k_\perp r) e^{i\Gamma\theta} \tag{6}$$

should be used. In (6), $\mathcal{C}_\Gamma(k_\perp r) = J_\Gamma(k_\perp r) + a_\Gamma Y_\Gamma(k_\perp r)$, where J_Γ and Y_Γ are Bessel functions of the first and second kind. The constants $\mathcal{C}_\Gamma$, a_Γ, and b_Γ depend on the tube geometry. For both of these eigenfunction basis sets the coordinate dependence is separable. The total time-averaged volume-integrated RF field energy stored in the fields $\mathcal{W}$ can in all cases be written as

$$\mathcal{W} = \frac{1}{16\pi} \int dV (\vec{E} \cdot \vec{E}^* + \vec{B} \cdot \vec{B}^*). \tag{7}$$

In calculating $\mathcal{W}$, any static magnetic field energy is not included.

We now consider the RF cavity fields for two specific cases, a slotted coaxial cylindrical cavity, as shown in Fig. 1(a), and a slotted rectangular cavity, as shown in Fig. 1(b). We will use N to designate the number of slots and L_z as the axial length of the cavity. In the cylindrical coaxial cavity, the central coaxial radius is given by R_i, while the inner and outer slot radii are respectively R and R_o. The angular width of the slots is taken to be $2\theta_o$. In the rectangular cavity, the inner and outer slot dimensions are R and R_o, while the cavity width in the x direction is given as L_x. The distance $2d$ between the slots equals twice the distance from the first or last slot to the tube wall; the slot width is taken to be $2w$. In the following, we make use of dimensionless units, with the cavity transverse length R being our scaling parameter. In these units, length is measured in units of R, time in units of R/c, frequency in units of c/R, and the background magnetic and RF fields are measured in units of $m_e c^2/|e|R$, where m_e is the electron rest mass, e is the electron charge, and c is the speed of light. The dimensionless cyclotron frequency Ω/γ is equal in these units to B_o/γ where B_o is the assumed constant background magnetic field and γ is the relativistic factor.

To determine the RF fields, it is convenient to treat the

cavity proper (Region I) and the slots (Region II) as separate expansions which are matched across the slot openings [21]. We take the relative phase dependence of each of the N slots as being $e^{i2\pi mq/N}$ for the cylindrical slotted case and $\cos[\pi(q + 1/2)m/N]$ for the rectangular slotted case, where $q = 0, \cdots, N - 1$ is the slot number. The value of the mode number m determines the overall mode. The 2π mode corresponds to $m = 0$, while the π mode is given by $m = N/2$ for a cylindrical slotted cavity, and by $m = N$ for a rectangular slotted cavity. In order to obtain a closed analytic form for the field solution, an infinite sum is used only in Region I, with just the $\Gamma = 0$ term being kept in Region II. The RF fields for the slotted coaxial cylindrical cavity are then given approximately by [12]

Region I

$$E_r = -E_o \frac{\omega}{k_\perp} \sum_{j=-\infty}^{\infty} \mathfrak{A}_\Gamma^I \left[\frac{\Gamma \mathfrak{C}_\Gamma^I(k_\perp r)}{k_\perp r}\right] \sin(k_z z) e^{i(\Gamma\theta - \omega t)} \quad (8)$$

$$E_\theta = -iE_o \frac{\omega}{k_\perp} \sum_{j=-\infty}^{\infty} \mathfrak{A}_\Gamma^I \mathfrak{C}_\Gamma^{I'}(k_\perp r) \sin(k_z z) e^{i(\Gamma\theta - \omega t)} \quad (9)$$

$$E_z = 0 \quad (10)$$

$$B_r = E_o \frac{k_z}{k_\perp} \sum_{j=-\infty}^{\infty} \mathfrak{A}_\Gamma^I \mathfrak{C}_\Gamma^{I'}(k_\perp r) \cos(k_z z) e^{i(\Gamma\theta - \omega t)} \quad (11)$$

$$B_\theta = iE_o \frac{k_z}{k_\perp} \sum_{j=-\infty}^{\infty} \mathfrak{A}_\Gamma^I \left[\frac{\Gamma \mathfrak{C}_\Gamma^I(k_\perp r)}{k_\perp r}\right] \cos(k_z z) e^{i(\Gamma\theta - \omega t)} \quad (12)$$

$$B_z = E_o \sum_{j=-\infty}^{\infty} \mathfrak{A}_\Gamma^I \mathfrak{C}_\Gamma^I(k_\perp r) \sin(k_z z) e^{i(\Gamma\theta - \omega t)} \quad (13)$$

Region II

$$E_r = 0 \quad (14)$$

$$E_\theta = -iE_o \frac{\omega}{k_\perp} e^{i2\pi mq/N} \mathfrak{A}_0^{II} \mathfrak{C}_0^{II'}(k_\perp r) \sin(k_z z) e^{-i\omega t} \quad (15)$$

$$E_z = 0 \quad (16)$$

$$B_r = E_o \frac{k_z}{k_\perp} e^{i2\pi mq/N} \mathfrak{A}_0^{II} \mathfrak{C}_0^{II'}(k_\perp r) \cos(k_z z) e^{-i\omega t} \quad (17)$$

$$B_\theta = 0 \quad (18)$$

$$B_z = E_o e^{i2\pi mq/N} \mathfrak{A}_0^{II} \mathfrak{C}_0^{II}(k_\perp r) \sin(k_z z) e^{-i\omega t} \quad (19)$$

where

$$\mathfrak{A}_\Gamma^I = \frac{\sin(\Gamma\theta_o)}{\Gamma} \frac{1}{\mathfrak{C}_\Gamma^{I'}(k_\perp)} \quad (20)$$

$$\mathfrak{A}_0^{II} = \frac{\pi}{N} \frac{1}{\mathfrak{C}_0^{II'}(k_\perp)} \quad (21)$$

and

$$\mathfrak{C}_\Gamma^I(k_\perp r) = J_\Gamma(k_\perp r) - J_\Gamma'(k_\perp R_i)\, Y_\Gamma(k_\perp r)/Y_\Gamma'(k_\perp R_i) \quad (22)$$

$$\mathfrak{C}_0^{II}(k_\perp r) = J_0(k_\perp r) - J_0'(k_\perp R_o)\, Y_0(k_\perp r)/Y_0'(k_\perp R_o). \quad (23)$$

A prime represents differentiation with respect to the argument. Due to the cavity symmetry, the only harmonics which contribute are $\Gamma = m + jN$, where $j = 0, \pm 1, \pm 2, \cdots$. For these fields, the dispersion relation determining $k_\perp$ and the total field energy $\mathfrak{W}$ are

$$\frac{N\theta_o}{\pi} \sum_{j=-\infty}^{\infty} \left(\frac{\sin\Gamma\theta_o}{\Gamma\theta_o}\right)^2 \frac{\mathfrak{C}_\Gamma^I(k_\perp)}{\mathfrak{C}_\Gamma^{I'}(k_\perp)} = \frac{\mathfrak{C}_0^{II}(k_\perp)}{\mathfrak{C}_0^{II'}(k_\perp)} \quad (24)$$

and

$$\mathfrak{W} = \frac{\omega^2 L_z}{k_\perp^2 16} \left\{ \sum_{j=-\infty}^{\infty} [\mathfrak{A}_\Gamma^I]^2 \left[[\mathfrak{C}_\Gamma^I(k_\perp)]^2 \left(1 - \frac{\Gamma^2}{k_\perp^2}\right) - R_i^2 [\mathfrak{C}_\Gamma^I(k_\perp R_i)]^2 \left(1 - \frac{\Gamma^2}{k_\perp^2 R_i^2}\right) + [\mathfrak{C}_\Gamma^{I'}(k_\perp)]^2 + \frac{1}{k_\perp} \mathfrak{C}_\Gamma^{I'}(k_\perp) \mathfrak{C}_\Gamma^I(k_\perp) \left(1 + \frac{k_z^2}{\omega^2}\right) \right] + \frac{N\theta_o [\mathfrak{A}_0^{II}]^2}{\pi} \left[R_o^2 [\mathfrak{C}_0^{II}(k_\perp R_o)]^2 - [\mathfrak{C}_0^{II}(k_\perp)]^2 - [\mathfrak{C}_0^{II'}(k_\perp)]^2 - \frac{1}{k_\perp} \mathfrak{C}_0^{II'}(k_\perp) \mathfrak{C}_0^{II}(k_\perp) \cdot \left(1 + \frac{k_z^2}{\omega^2}\right) \right] \right\}. \quad (25)$$

The slight difference between $\mathfrak{W}$ as given in (25) and the form presented by Chu and Dialetis [11], [12] stems from our use of the field energy density $\vec{E} \cdot \vec{E}^* + \vec{B} \cdot \vec{B}^*$ while Chu and Dialetis used $2\vec{E} \cdot \vec{E}^*$. If the RF fields were calculated exactly, with an infinite series expansion for both Regions I and II, then the energy in the magnetic fields would equal that in the electric fields and both expressions for $\mathfrak{W}$ would be identical.

The rectangular slotted fields (see, e.g., [18] for a derivation) for our tube are

Region I

$$E_x = -i \frac{\omega}{k_\perp^2} E_o \sum_\Gamma k_{y\Gamma} \mathfrak{A}_\Gamma^I \cos(k_{x\Gamma} x) \cdot \sin(k_{y\Gamma} y) \sin(k_z z) e^{-i\omega t} \quad (26)$$

$$E_y = i \frac{\omega}{k_\perp^2} E_o \sum_\Gamma k_{x\Gamma} \mathfrak{A}_\Gamma^I \sin(k_{x\Gamma} x) \cdot \cos(k_{y\Gamma} y) \sin(k_z z) e^{-i\omega t} \quad (27)$$

$$E_z = 0 \quad (28)$$

$$B_x = -\frac{k_z}{k_\perp^2} E_o \sum_\Gamma k_{x\Gamma} \mathfrak{A}_\Gamma^I \sin(k_{x\Gamma}x) \cdot \cos(k_{y\Gamma}y) \cos(k_z z) e^{-i\omega t} \quad (29)$$

$$B_y = -\frac{k_z}{k_\perp^2} E_o \sum_\Gamma k_{y\Gamma} \mathfrak{A}_\Gamma^I \cos(k_{x\Gamma}x) \cdot \sin(k_{y\Gamma}y) \cos(k_z z) e^{-i\omega t} \quad (30)$$

$$B_z = E_o \sum_\Gamma \mathfrak{A}_\Gamma^I \cos(k_{x\Gamma}x) \cos(k_{y\Gamma}y) \sin(k_z z) e^{-i\omega t} \quad (31)$$

Region II

$$E_x = -i\frac{\omega}{k_\perp} E_o \cos\left(\pi(q + 1/2)m/N\right)\mathfrak{A}_0^{II} \cdot \sin(k_\perp y) \sin(k_z z) e^{-i\omega t} \quad (32)$$

$$E_y = 0 \quad (33)$$

$$E_z = 0 \quad (34)$$

$$B_x = 0 \quad (35)$$

$$B_y = -\frac{k_z}{k_\perp} E_o \cos\left(\pi(q + 1/2)m/N\right)\mathfrak{A}_0^{II} \cdot \sin(k_\perp y) \cos(k_z z) e^{-i\omega t} \quad (36)$$

$$B_z = E_o \cos\left(\pi(q + 1/2)m/N\right)\mathfrak{A}_0^{II} \cdot \cos(k_\perp y) \sin(k_z z) e^{-i\omega t} \quad (37)$$

where $k_{x\Gamma} = \Gamma\pi/L_x$, $k_{y\Gamma} = (k_\perp^2 - k_{x\Gamma}^2)^{1/2}$, and

$$\mathfrak{A}_\Gamma^I = \frac{2k_\perp^2 \sin(k_{x\Gamma}w)(-1)^j}{(1 + \delta_{\Gamma 0})k_{x\Gamma}k_{y\Gamma} \sin(k_{y\Gamma})} \quad (38)$$

$$\mathfrak{A}_0^{II} = \frac{k_\perp L_x}{N \sin\left[k_\perp(1 - R_o)\right]}. \quad (39)$$

Only $\Gamma = \pm m + 2Nj$, $j = 0, 1, 2, \cdots$, with $\Gamma \geq 0$, are to be included in the sums. For $m = 0$, each term for $\Gamma = 2Nj$ must be counted twice. For our model of a rectangular slotted cavity, the RF field in Region I is not affected by the presence of the slots for the modes $m = Ni$, where $i = 1, 3, 5, \cdots$, and has the same form as in a simple smooth-walled cavity. For all other rectangular cavity modes, the dispersion relation for $k_\perp$ and volume-integrated energy $\mathfrak{W}$ can be written as

$$\frac{2Nw}{L_x} \sum_\Gamma \frac{k_\perp}{1 + \delta_{\Gamma 0}} \left[\frac{\sin(k_{x\Gamma}w)}{k_{x\Gamma}w}\right]^2 \frac{\cot(k_{y\Gamma})}{k_{y\Gamma}} = \cot\left[k_\perp(1 - R_o)\right] \quad (40)$$

and

$$\mathfrak{W} = \frac{L_z L_x \omega^2 (1 + \delta_{m0})}{64\pi k_\perp^2} \left(\sum_\Gamma (\mathfrak{A}_\Gamma^I)^2 (1 + \delta_{\Gamma 0}) \cdot \left\{ 1 + \frac{\sin(2k_{y\Gamma})}{4k_{y\Gamma}} \left[\frac{k_\perp^2}{\omega^2} + \left(1 + \frac{k_z^2}{\omega^2}\right) \cdot \left(\frac{2k_{x\Gamma}^2}{k_\perp^2} - 1\right)\right]\right\} + \frac{2Nw(R_o - 1)(\mathfrak{A}_0^{II})^2}{L_x} \cdot \left[1 + \frac{\sin\left(2k_\perp(1 - R_o)\right)}{4k_\perp(1 - R_o)} \left(\frac{k_\perp^2}{\omega^2} - 1 - \frac{k_z^2}{\omega^2}\right)\right]\right). \quad (41)$$

III. Linear Kinetic Theory

To solve for the interaction of the electron beam with the RF field, we use the single-particle relativistic equation of motion:

$$\frac{d\vec{U}}{dz} = -\frac{\gamma}{U_z}\left[\vec{E} + \frac{\vec{U} \times \vec{B}}{\gamma}\right] \quad (42)$$

where $\vec{U} = \gamma\vec{\beta}$ is the product of the electron velocity $\vec{\beta}$ and the Lorentz factor γ. Note that we are using time $t(z)$ as a dependent variable and the axial position z as the independent variable. The use of z facilitates the comparison of the linear theory with the weak field limit of a nonlinear numerical modeling of the equations of motion. In dimensionless units, $\gamma = (1 + \vec{U} \cdot \vec{U})^{1/2} = (1 + U_z^2 + U_\perp^2)^{1/2}$ gives the electron energy. From (42) it follows that the change in γ is

$$\frac{d\gamma}{dz} = -\frac{\vec{U} \cdot \vec{E}}{U_z}. \quad (43)$$

Regardless of the symmetry of the overall cavity fields, the guiding-center coordinates (see Fig. 2) are the natural system to use when carrying our linear theory. The guiding-center variables may be expressed as $(U_\perp, U_z, \varphi, x_{gc}, y_{gc}, t)$ in Cartesian coordinates or $(U_\perp, U_z, \varphi, r_{gc}, \psi_{gc}, t)$ in cylindrical coordinates. The guiding-center coordinates are related to cavity-frame coordinates by the relations

$$x = x_{gc} + r_L \cos(\varphi) = r_{gc} \cos(\psi_{gc}) + r_L \cos(\varphi) \quad (44)$$

$$y = y_{gc} + r_L \sin(\varphi) = r_{gc} \sin(\psi_{gc}) + r_L \sin(\varphi) \quad (45)$$

$$U_x = -U_\perp \sin(\varphi) \quad (46)$$

$$U_y = U_\perp \cos(\varphi). \quad (47)$$

The position (x_{gc}, y_{gc}) or (r_{gc}, ψ_{gc}) corresponds to the electron-guiding-center position, with $r_L = U_\perp/B_o$ being the Larmor radius. The dynamical equations for the guid-

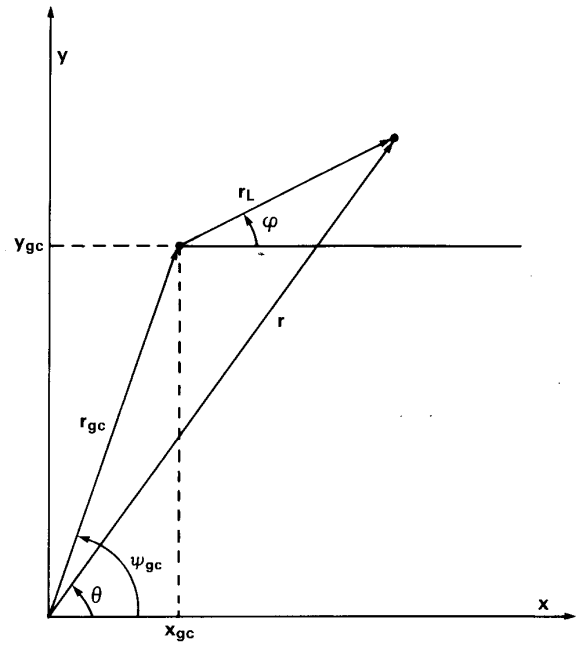

Fig. 2. Guiding-center coordinate system.

ing-center variables follow from (42) and (44)–(47):

$$\frac{dU_\perp}{dz} = -\frac{\gamma}{U_z}\left[E_\varphi + U_z B_{r_L}/\gamma\right] \tag{48}$$

$$\frac{d\varphi}{dz} = \frac{\gamma}{U_z U_\perp}\left[E_{r_L} - U_z B_\varphi/\gamma + U_\perp B_z/\gamma\right] + \frac{B_o}{U_z} \tag{49}$$

$$\frac{dU_z}{dz} = \frac{U_\perp}{U_z} B_{r_L} \tag{50}$$

$$\frac{dt}{dz} = \frac{\gamma}{U_z} \tag{51}$$

and either

$$\frac{dx_{gc}}{dz} = \frac{\gamma}{U_z B_o}\left[(E_\varphi + U_z B_{r_L}/\gamma)\cos(\varphi) + (E_{r_L} - U_z B_\varphi/\gamma + U_\perp B_z/\gamma)\sin(\varphi)\right] \tag{52}$$

$$\frac{dy_{gc}}{dz} = \frac{\gamma}{U_z B_o}\left[(E_\varphi + U_z B_{r_L}/\gamma)\sin(\varphi) - (E_{r_L} - U_z B_\varphi/\gamma + U_\perp B_z/\gamma)\cos(\varphi)\right] \tag{53}$$

or

$$\frac{dr_{gc}}{dz} = \frac{\gamma}{U_z B_o}\left[(E_\varphi + U_z B_{r_L}/\gamma)\cos(\psi_{gc} - \varphi) - (E_{r_L} - U_z B_\varphi/\gamma + U_\perp B_z/\gamma)\sin(\psi_{gc} - \varphi)\right] \tag{54}$$

$$\frac{d\psi_{gc}}{dz} = -\frac{\gamma}{r_{gc} U_z B_o}\left[(E_\varphi + U_z B_{r_L}/\gamma)\sin(\psi_{gc} - \varphi) + (E_{r_L} - U_z B_\varphi/\gamma + U_\perp B_z/\gamma)\cos(\psi_{gc} - \varphi)\right]. \tag{55}$$

The RF fields terms, E_φ, E_{r_L}, B_φ, and B_{r_L}, correspond to the values of $\vec{E}$ and $\vec{B}$ along the $\hat{\varphi}$ and $\hat{r}_L$ directions.

To solve for the perturbations induced by the RF field, we linearize the equations of motion as follows:

$$U_\perp = U_{\perp o} + \delta U_\perp \tag{56}$$

$$U_z = U_{z_o} + \delta U_z \tag{57}$$

$$\varphi = \varphi_o + B_o \frac{(z - z_o)}{U_{z_o}} + \delta\varphi \tag{58}$$

$$x_{gc} = x_{gc_o} + \delta x_{gc} \tag{59}$$

$$y_{gc} = y_{gc_o} + \delta y_{gc} \tag{60}$$

$$r_{gc} = r_{gc_o} + \delta r_{gc} \tag{61}$$

$$\psi_{gc} = \psi_{gc_o} + \delta\psi_{gc} \tag{62}$$

$$t = t_o + \frac{\gamma_o (z - z_o)}{U_{z_o}} + \delta t \tag{63}$$

where the constants $U_{\perp o}$, U_{z_o}, φ_o, x_{gc_o}, y_{gc_o}, r_{go_o}, ψ_{gc_o}, and t_o represent the initial variable values at the entrance position of the cavity z_o. In the following we take $z_o = 0$. The equations of motion for the perturbed variables then follow as

$$\frac{d\delta U_\perp}{dz} = -\frac{\gamma_o}{U_{z_o}} \tilde{E}^o_\varphi \tag{64}$$

$$\frac{d\delta\varphi}{dz} = \frac{\gamma_o}{U_{z_o} U_{\perp o}} \tilde{E}^o_{r_L} - B_o \frac{\delta U_z}{U^2_{z_o}} \tag{65}$$

$$\frac{d\delta U_z}{dz} = \frac{U_{\perp o}}{U_{z_o}} B^o_{r_L} \tag{66}$$

$$\frac{d\delta t}{dz} = -\frac{1}{\gamma_o U_{z_o}}\left[\frac{1 + U^2_{\perp o}}{U_{z_o}} \delta U_z - U_{\perp o}\delta U_{\perp o}\right] \tag{67}$$

$$\frac{d\delta x_{gc}}{dz} = \frac{\gamma_o}{U_{z_o} B_o}\left[\tilde{E}^o_\varphi \cos(\phi_o) + \tilde{E}^o_{r_L} \sin(\phi_o)\right] \tag{68}$$

$$\frac{d\delta y_{gc}}{dz} = \frac{\gamma_o}{U_{z_o} B_o}\left[\tilde{E}^o_\varphi \sin(\phi_o) - \tilde{E}^o_{r_L} \cos(\phi_o)\right] \tag{69}$$

$$\frac{d\delta r_{gc}}{dz} = \frac{\gamma_o}{U_{z_o} B_o}\left[\tilde{E}^o_\varphi \cos(\psi_{gc_o} - \phi_o) - \tilde{E}^o_{r_L} \sin(\psi_{gc_o} - \phi_o)\right] \tag{70}$$

$$\frac{d\delta\psi_{gc}}{dz} = -\frac{\gamma_o}{U_{z_o}B_o r_{gc_o}}\left[\tilde{E}^o_\varphi \sin(\psi_{gc_o} - \phi_o) + \tilde{E}^o_{r_L}\cos(\psi_{gc_o} - \phi_o)\right] \quad (71)$$

where

$$\tilde{E}^o_\varphi = E^o_\varphi + U_{z_o}B^o_{r_L}/\gamma_o \quad (72)$$

$$\tilde{E}^o_{r_L} = E^o_{r_L} - U_{z_o}B^o_\varphi/\gamma_o + U^o_\perp B^o_z/\gamma_o \quad (73)$$

$$\phi_o = \varphi_o + B_o z/U_{z_o}. \quad (74)$$

E^o_φ, $E^o_{r_L}$, B^o_φ, $B^o_{r_L}$, and B^o_z are the RF field terms in the $\hat{\varphi}$, $\hat{r}_L$, and $\hat{z}$ directions evaluated along the unperturbed orbits. $\tilde{E}^o_\varphi$ and $\tilde{E}^o_{r_L}$ represent, respectively, the $\hat{\varphi}$ and $\hat{r}_L$ components of vector $\vec{E} + \vec{U}\times\vec{B}/\gamma$ from the equation of motion also evaluated along the unperturbed orbits. The variable ϕ_o gives the phase variation about the guiding center for zero RF field.

To calculate the average change in energy for the beam, we must also linearize the energy equation, (43), which becomes

$$\frac{d\delta\gamma}{dz} = -\frac{\delta U_\perp}{U_{z_o}}E^{o*}_\varphi + \frac{U_{\perp_o}\delta U_z}{U^2_{z_o}}E^{o*}_\varphi - \frac{U_{\perp_o}}{U_{z_o}}\left[\delta t\frac{\partial E^{o*}_\varphi}{\partial t} + \delta r_{gc}\frac{\partial E^{o*}_\varphi}{\partial r_{gc}} + \delta\psi_{gc}\frac{\partial E^{o*}_\varphi}{\partial\psi_{gc}} + \delta r_L\frac{\partial E^{o*}_\varphi}{\partial r_L} + \delta\varphi\frac{\partial E^{o*}_\varphi}{\partial\varphi}\right] \quad (75)$$

or

$$\frac{d\delta\gamma}{dz} = -\frac{\delta U_\perp}{U_{z_o}}E^{o*}_\varphi + \frac{U_{\perp_o}\delta U_z}{U^2_{z_o}}E^{o*}_\varphi - \frac{U_{\perp_o}}{U_{z_o}}\left[\delta t\frac{\partial E^{o*}_\varphi}{\partial t} + \delta x_{gc}\frac{\partial E^{o*}_\varphi}{\partial x_{gc}} + \delta y_{gc}\frac{\partial E^{o*}_\varphi}{\partial y_{gc}} + \delta r_L\frac{\partial E^{o*}_\varphi}{\partial r_L} + \delta\varphi\frac{\partial E^{o*}_\varphi}{\partial\varphi}\right]. \quad (76)$$

For a constant background magnetic field B_o, $\delta r_L = \delta U_\perp/B_o$. The equations for $d\delta\gamma/dz$ have been expanded to second order in the RF field amplitude E_o.

In order to solve these linearized equations, we must express the RF fields in terms of the guiding-center coordinates. For the cylindrical geometry eigenfunction set (8)–(13), Graf's theorem is used to give [22]

$$\mathcal{C}_\nu(k_\perp r)^{\cos}_{\sin}\nu(\psi_{gc} - \theta) = \sum_{k=-\infty}^{\infty}\mathcal{C}_{\nu+k}(\mathcal{K}_{gc})J_k(\mathcal{K}_L)^{\cos}_{\sin}k(\pi - \psi_{gc} + \varphi) \quad (77)$$

for $r_{gc} > r_L$, or

$$\mathcal{C}_\nu(k_\perp r)^{\cos}_{\sin}\nu(\psi_{gc} - \theta) = \sum_{k=-\infty}^{\infty}J_{\nu+k}(\mathcal{K}_{gc})\,\mathcal{C}_k(\mathcal{K}_L)^{\cos}_{\sin}k(\pi - \psi_{gc} + \varphi) \quad (78)$$

for $r_{gc} < r_L$, where $\mathcal{K}_{gc} = k_\perp r_{gc}$ and $\mathcal{K}_L = k_\perp r_L$. For the rectangular geometry eigenfunction set (26)–(31), the expansions

$$\cos[\mathcal{K}_L\sin(\varphi \pm \lambda)] = \sum_{k=-\infty}^{\infty}J_k(\mathcal{K}_L)\cos[k(\varphi \pm \lambda)] \quad (79)$$

$$\sin[\mathcal{K}_L\sin(\varphi \pm \lambda)] = \sum_{k=-\infty}^{\infty}J_k(\mathcal{K}_L)\sin[k(\varphi \pm \lambda)] \quad (80)$$

$$\cos[\mathcal{K}_L\cos(\varphi \pm \lambda)] = \sum_{k=-\infty}^{\infty}J_k(\mathcal{K}_L)\cos[k(\varphi \pm \lambda + \pi/2)] \quad (81)$$

$$\sin[\mathcal{K}_L\cos(\varphi \pm \lambda)] = \sum_{k=-\infty}^{\infty}J_k(\mathcal{K}_L)\sin[k(\varphi \pm \lambda + \pi/2)] \quad (82)$$

are similarly used. In (79)–(82), $\cos\lambda = k_x/k_\perp$.

Using the above expansions, the guiding-center RF fields in Region I, which contains the beam, can be expressed as

$$E_{r_L} = -\frac{\omega}{k_\perp}E_o\sum_\Gamma\mathcal{A}^I_\Gamma\sum_{s=-\infty}^{\infty}\mathcal{D}_{\Gamma s}\left(\frac{sJ_s(\mathcal{K}_L)}{\mathcal{K}_L}\right)\cdot\sin(k_z z)\,e^{i(s\varphi-\omega t)} \quad (83)$$

$$E_\varphi = -i\frac{\omega}{k_\perp}E_o\sum_\Gamma\mathcal{A}^I_\Gamma\sum_{s=-\infty}^{\infty}\mathcal{D}_{\Gamma s}J'_s(\mathcal{K}_L)\cdot\sin(k_z z)\,e^{i(s\varphi-\omega t)} \quad (84)$$

$$B_{r_L} = \frac{k_z}{\omega}E_o\sum_\Gamma\mathcal{A}^I_\Gamma\sum_{s=-\infty}^{\infty}\mathcal{D}_{\Gamma s}J'_s(\mathcal{K}_L)\cos(k_z z)\,e^{i(s\varphi-\omega t)} \quad (85)$$

$$B_\varphi = i\frac{k_z}{\omega}E_o\sum_\Gamma\mathcal{A}^I_\Gamma\sum_{s=-\infty}^{\infty}\mathcal{D}_{\Gamma s}\left(\frac{sJ_s(\mathcal{K}_L)}{\mathcal{K}_L}\right)\cdot\cos(k_z z)\,e^{i(s\varphi-\omega t)} \quad (86)$$

$$B_z = E_o\sum_\Gamma\mathcal{A}^I_\Gamma\sum_{s=-\infty}^{\infty}\mathcal{D}_{\Gamma s}J_s(\mathcal{K}_L)\sin(k_z z)\,e^{i(s\varphi-\omega t)} \quad (87)$$

where the function $\mathfrak{D}_{\Gamma s}$ is

$$\mathfrak{D}_{\Gamma s} = \mathcal{C}^{I}_{\Gamma - s}(\mathcal{K}_{gc})\, e^{i(\Gamma - s)\psi_{gc}} \tag{88}$$

for the cylindrical coordinates eigenfunction expansion, and

$$\mathfrak{D}_{\Gamma s} = \tfrac{1}{2}\left[e^{ik_{x\Gamma}x_{gc}} \cos\left(k_{y\Gamma}y_{gc} - s\lambda_{\Gamma}\right) + (-1)^{s} e^{-ik_{x\Gamma}x_{gc}} \cos\left(k_{y\Gamma}y_{gc} + s\lambda_{\Gamma}\right)\right] e^{is\pi/2} \tag{89}$$

for the Cartesian coordinates expansion. For cylindrical coordinates, if $r_L > r_{gc}$, the replacement $\mathcal{C}^{I} \to J$ and $J \to \mathcal{C}^{I}$ must be made in (83)–(88). The form of the guiding-center RF fields is clearly independent of the choice of the coordinate eigenfunction-basis set one wishes to use to describe the cavity fields, and follows from the Fourier transformation for our separable eigenfunction expansion. To determine the contribution of the cavity field at the sth harmonic, one merely sums the contribution from each Γ eigenfunction $\mathfrak{A}^{I}_{\Gamma}\mathfrak{D}_{\Gamma s}$.

When evaluated along the unperturbed particle orbits, the only variation in the guiding-center RF fields (83)–(87) comes from $\sin(k_z z)\, e^{i(s\varphi - \omega t)}$, which takes the simple form $(e^{ik_z z} - e^{-ik_z z})\, e^{i(sB_o/\gamma_o - \omega)\gamma_o z/U_{z_o}}\, e^{i(s\varphi_o - \omega t_o)}/2i$, making the linearized equations of motion simple to evaluate. These equations are solved in the following order: We first integrate (64), (66), (68), and (69), or (64), (66), (70), and (71), to determine $\delta U_{\perp}$, δU_z, and either δx_{gc} and δy_{gc} or δr_{gc} and $\delta\psi_{gc}$. The expressions for $\delta U_{\perp}$ and δU_z are then substituted into (65) and (67) to determine $\delta\varphi$ and δt. Using these perturbed orbital variables, (75) or (76) is finally integrated from $z = 0$ to $z = L$ in order to calculate $\delta\gamma$. The perturbed energy change is then averaged over t_o and the phase angle φ_o. We will not average over guiding-center position at this point. The averaged form for $\langle \delta\gamma \rangle_{t_o\varphi_o}$, which comes from a straightforward integration of (75) or (76), is given by

$$\langle \delta\gamma \rangle_{t_o\varphi_o} = -\frac{E_o^2\gamma_o\omega^2}{8U_{z_o}^2k_{\perp}^2} \sum_{\Gamma}\sum_{\Lambda} \mathfrak{A}^{I*}_{\Gamma}\mathfrak{A}^{I}_{\Lambda} \cdot \sum_{s=-\infty}^{\infty} (\alpha_1 + \alpha_2 + \alpha_3 + \alpha_4) \tag{90}$$

where

$$\alpha_1 = \frac{U_{\perp_o}^2L_z^3}{\gamma_o U_{z_o}\omega\mu_-^3}(\omega^2 - k_z^2)\left[i\mu_-(e^{i\mu_-} + 1) - 2(e^{i\mu_-} - 1)\right]H_{\Gamma\Lambda s} - \frac{U_{\perp_o}^2L_z^2k_z}{\gamma_o U_{z_o}\omega\mu_-^2}\left[i\mu_- e^{i\mu_-} - e^{i\mu_-} + 1\right]H_{\Gamma\Lambda s} - \frac{L_z^2}{\omega\mu_-^2}(i\mu_- - e^{i\mu_-} + 1) \cdot \left[(\omega - k_zU_{z_o}/\gamma_o)\,T_{\Gamma\Lambda s} - k_{\perp}U_{\perp_o}U_{\Gamma\Lambda s}/\gamma_o\right] \tag{91}$$

$$\alpha_4 = -\frac{U_{\perp_o}^2L_z^3}{\gamma_o U_{z_o}\omega\mu_-\mu_+^2}(\omega^2 - k_z^2)\left[(i\mu_- e^{i\mu_-} - e^{i\mu_-} + 1) \cdot \frac{\mu_+}{\mu_-} - e^{i\mu_-} + 1\right]H_{\Gamma\Lambda s} - \frac{U_{\perp_o}^2L_z^2k_z}{\gamma_o U_{z_o}\omega\mu_-^2}\left[i\mu_- e^{i\mu_-} - e^{i\mu_-} + 1\right]H_{\Gamma\Lambda s} - \frac{L_z^2}{\omega\mu_+\mu_-}(e^{i\mu_-} - 1) \cdot \left[(\omega + k_zU_{z_o}/\gamma_o)T_{\Gamma\Lambda s} - k_{\perp}U_{\perp_o}U_{\Gamma\Lambda s}/\gamma_o\right] \tag{92}$$

$$\mu_{\pm} = (\omega - sB_o/\gamma_o \pm k_zU_{z_o}/\gamma_o)L_z\gamma_o/U_{z_o} \tag{93}$$

and

$$H_{\Gamma\Lambda s} = \mathfrak{D}^{*}_{\Gamma s}\mathfrak{D}_{\Lambda s}\left[J_s'(\mathcal{K}_{L_o})\right]^2 \tag{94}$$

$$T_{\Gamma\Lambda s} = H_{\Gamma\Lambda s} + \mathcal{K}_{L_o}J_s'(\mathcal{K}_{L_o})\left\{J_s''(\mathcal{K}_{L_o})\mathfrak{D}^{*}_{\Gamma s}\mathfrak{D}_{\Lambda s} - J_s(\mathcal{K}_{L_o})\frac{\left[\mathfrak{D}^{*}_{\Gamma s+1}\mathfrak{D}_{\Lambda s+1} + \mathfrak{D}^{*}_{\Gamma s-1}\mathfrak{D}_{\Lambda s-1}\right]}{2} + \frac{s^2J_s(\mathcal{K}_{L_o})\,\mathfrak{D}^{*}_{\Gamma s}D_{\Lambda s}}{\mathcal{K}_o^2}\right\} \tag{95}$$

$$U_{\Gamma\Lambda s} = -\frac{\mathcal{K}_{L_o}J_s'(\mathcal{K}_{L_o})}{2}\left\{J_{s-1}(\mathcal{K}_{L_o}) \cdot \left[\mathfrak{D}^{*}_{\Gamma s-1}\mathfrak{D}_{\Lambda s-1} - \mathfrak{D}^{*}_{\Gamma s}\mathfrak{D}_{\Lambda s}\right] + J_{s+1}(\mathcal{K}_{L_o}) \cdot \left[\mathfrak{D}^{*}_{\Gamma s+1}\mathfrak{D}_{\Lambda s+1} - \mathfrak{D}^{*}_{\Gamma s}\mathfrak{D}_{\Lambda s}\right]\right\}. \tag{96}$$

The functions α_2 and α_3 are related to α_1 and α_4 by

$$\alpha_2(k_z) = \alpha_1(-k_z) \tag{97}$$

$$\alpha_3(k_z) = \alpha_4(-k_z). \tag{98}$$

Equation (90) for $\langle \delta\gamma \rangle_{t_o\varphi_o}$ contains a double sum over the cavity mode harmonics Γ and Λ. For the cylindrical coordinates expansion, Γ and Λ are restricted to $\Gamma = Nj + m$ for $j = 0, \pm1, \pm2, \cdots$ and $\Lambda = Nk + m$ for $k = 0, \pm1, \pm2, \cdots$. For the Cartesian coordinates expansion, the nonnegative harmonics which satisfy $\Gamma = 2Nj \pm m$, where $j = 0, 1, 2, \cdots$, and $\Lambda = 2Nk \pm m$, where $k = 0, 1, 2, \cdots$, are allowed. When $m = 0$, the two Cartesian Γ cavity mode harmonics $\Gamma = 2Nj + m$ and $\Gamma = 2Nj - m$, and two Λ cavity mode harmonics $\Lambda = 2Nk + m$ and $\Lambda = 2Nk - m$ are identical. In this case, the sums over Γ or Λ can be written as twice the sum for all $\Gamma = 2Nj$ or $\Lambda = 2Nk$. Note again that for the cylindrical expansion, if $r_{L_o} > r_{gc_o}$ one must make the replacement $\mathcal{C}^{I} \to J$ and $J \to \mathcal{C}^{I}$ in the above relations.

In (90), the variation of $\langle \delta\gamma \rangle_{t_o\varphi_o}$ with guiding-center position only enters through the factors $\mathfrak{D}^{*}_{\Gamma s}\mathfrak{D}_{\Lambda s}$,

$\mathfrak{D}^*_{\Gamma s+1}\mathfrak{D}_{\Lambda s+1}$, and $\mathfrak{D}^*_{\Gamma s-1}\mathfrak{D}_{\Lambda s-1}$. Averaging over the guiding-center position ψ_{gc_o} from 0 to π for the cylindrical case, or x_{gc_o} from 0 to L_x for the Cartesian coordinate case, collapses the double sum over Γ and Λ to a single sum with $\Gamma = \Lambda$ and $\mathfrak{D}_{\Gamma k}\mathfrak{D}^*_{\Gamma k}$ replaced by either $[\mathfrak{C}^I_{\Gamma -k}]^2$ or $[\cos(k_{y\Gamma}y_{gc_o})^2\cos(s\lambda_\Gamma)^2 + \sin(k_{y\Gamma}y_{gc_o})^2\sin(s\lambda_\Gamma)^2]/2$. For the cylindrical slotted gyrotron oscillator, the resulting expression for $\langle \delta\gamma\rangle_{t_o\varphi_o\psi_{gc_o}}$ agrees with the results of Chu and Dialetis [11], [12]. While this guiding-center averaging is reasonable for modeling an axisymmetric beam in a cylindrical cavity, it is not reasonable in a rectangular cavity, where x_{gc_o} cannot realistically be taken within r_{L_o} of the cavity walls. If $m = 2Ni$ where $i = 0, 1, 2, \cdots$, then the RF field shows an N-fold periodicity in the x direction, and the simplifying x_{gc_o} averaging can be done from $L_x(j/N)$ to $L_x(k/N)$, where $0 < j < N-1$, and $j < k < N$.

The form of $\langle \delta\gamma\rangle_{t_o\varphi_o}$ given in (90) is a very complicated function of the beam and cavity parameters. It is far from the most compact form for the net energy change, and it does not clearly show the separate contributions from the electron cyclotron maser interaction, the peniotron interaction, and other interactions. A more compact form can be obtained by combining and rearranging the terms in $\alpha_1 + \alpha_2 + \alpha_3 + \alpha_4$. To begin we will rewrite $\langle \delta\gamma\rangle_{t_o\varphi_o}$ in the form

$$\langle \delta\gamma\rangle_{t_o\varphi_o} = \frac{E_o^2\gamma_o\omega^2}{k_z^2U_{z_o}^2k_\perp^2}\sum_\Gamma\sum_\Lambda \mathfrak{A}^{I*}_\Gamma\mathfrak{A}^I_\Lambda \cdot \sum_{s=-\infty}^{\infty}\left\{\left[\frac{s\Omega}{\gamma_o\omega}T_{\Gamma\Lambda s} - \frac{k_\perp U_{\perp_o}}{\gamma_o\omega}U_{\Gamma\Lambda s}\right]\mathcal{G} + \frac{2\lambda k_z U_{\perp_o}^2}{\gamma_o U_{z_o}\omega}H_{\Gamma\Lambda s}\mathcal{G} - \frac{U_{\perp_o}^2}{\gamma_o U_{z_o}k_z\omega}\cdot[\omega^2 - k_z^2\lambda^2]H_{\Gamma\Lambda s}\mathcal{G}' + i\frac{k_zL_z}{4\omega}\left[\frac{U_{\perp_o}^2k_z}{\gamma_oU_{z_o}}H_{\Gamma\Lambda s} + \frac{k_zU_{z_o}}{\gamma_o}T_{\Gamma\Lambda s}\right]\right\} \tag{99}$$

where

$$\lambda = \left(\frac{s\Omega}{\gamma_o} - \omega\right)\frac{\gamma_o}{k_zU_{z_o}} \tag{100}$$

$$\mathcal{G} = \frac{e^{-i[l\pi\lambda + (l-1)\pi]} + 1}{2(\lambda^2-1)^2} - i\frac{l\pi\lambda}{4(\lambda^2-1)}. \tag{101}$$

While (99) shows explicitly the rapid variations in the magnetic mistuning variable λ about the harmonic resonances, one can still obtain a simpler form for $\langle \delta\gamma\rangle_{t_o\varphi_o}$. Upon expanding and rewriting the $H_{\Gamma\Lambda s}$, $T_{\Gamma\Lambda s}$, and $U_{\Gamma\Lambda s}$ terms, the following final expression can be obtained:

$$\begin{aligned}\langle \delta\gamma\rangle_{t_o\varphi_o} = &-\frac{E_o^2\gamma_o\omega^2}{k_z^2U_{z_o}^2k_\perp^2}\sum_{s=-\infty}^{\infty}\sum_\Gamma \mathfrak{A}^{I*}_\Gamma\mathfrak{D}^*_{\Gamma s}\sum_\Lambda\mathfrak{A}^I_\Lambda\mathfrak{D}_{\Lambda s}\\ &\cdot\left\{\frac{U_{\perp_o}^2J_s'^2(\mathcal{K}_{L_o})}{\gamma_oU_{z_o}}\left(\frac{\omega}{k_z}\frac{dg(\lambda)}{d\lambda} - \frac{k_z}{\omega}\frac{d\lambda^2g(\lambda)}{d\lambda}\right)\right.\\ &-2sJ_s'(\mathcal{K}_{L_o})\left(\frac{sJ_s(\mathcal{K}_{L_o})}{\mathcal{K}_{L_o}}\frac{s\Omega}{\gamma_o\omega}\right.\\ &\left.-\frac{k_\perp U_{\perp_o}}{\gamma_o\omega}J_s(\mathcal{K}_{L_o})\right)g(\lambda) - \frac{k_\perp^2U_{\perp_o}^2}{2\gamma_o\Omega\omega}\\ &\cdot[J_{s+1}'^2(\mathcal{K}_{L_o})g(\lambda^+) - J_{s-1}'^2(\mathcal{K}_{L_o})g(\lambda^-)]\\ &-i\frac{k_zL_z}{4}\left[\frac{U_{\perp_o}^2J_s'^2(\mathcal{K}_{L_o})}{\gamma_oU_{z_o}}\left(\frac{\omega}{k_z}\frac{df(\lambda)}{d\lambda}\right.\right.\\ &\left.-\frac{k_z}{\omega}\frac{d\lambda^2f(\lambda)}{d\lambda} + \frac{k_z}{\omega}\right)\\ &-2sJ_s'(\mathcal{K}_{L_o})\left(\frac{sJ_s(\mathcal{K}_{L_o})}{\mathcal{K}_{L_o}}\right.\\ &\cdot\left[\frac{k_zU_{z_o}}{\gamma_o\omega}(\lambda f(\lambda) - 1) + f(\lambda)\right] - \frac{k_\perp U_{\perp_o}}{\gamma_o\omega}J_s\\ &\left.\cdot(\mathcal{K}_{L_o})f(\lambda)\right) - \frac{k_\perp U_{\perp_o}}{2\gamma_o\Omega\omega}\left[k_\perp U_{\perp_o}(J_{s+1}'^2(\mathcal{K}_{L_o})\right.\\ &\cdot f(\lambda^+) - J_{s-1}'^2(\mathcal{K}_{L_o})f(\lambda^-)) + k_zU_{z_o}\\ &\cdot\left(J_{s+1}(\mathcal{K}_{L_o})J_{s+1}'(\mathcal{K}_{L_o}) + J_{s-1}(\mathcal{K}_{L_o})\right.\\ &\left.\left.\left.\cdot J_{s-1}'(\mathcal{K}_{L_o}) + 2J_s(\mathcal{K}_{L_o})J_s'(\mathcal{K}_{L_o})\right)\right]\right\}\end{aligned} \tag{102}$$

where

$$g = \left(\frac{\cos(\mu)}{(\lambda^2-1)}\right)^2 \tag{103}$$

$$f = \frac{\lambda}{(\lambda^2-1)} + \frac{4\sin(\mu)\cos(\mu)}{k_zL_z(\lambda^2-1)^2} \tag{104}$$

$$\lambda^\pm = \left(\frac{(s\pm1)\Omega}{\gamma_o} - \omega\right)\frac{\gamma_o}{k_zU_{z_o}} \tag{105}$$

$$\mu = l\pi\lambda/2 + (l-1)\pi/2. \tag{106}$$

Because the product $\Sigma_\Gamma\mathfrak{A}^{I*}_\Gamma\mathfrak{D}^*_{\Gamma s}\Sigma_\Lambda\mathfrak{A}^I_\Lambda\mathfrak{D}_{\Lambda s}$ is real, and since all of the variables and functions within the brackets $\{\cdots\}$ are real, the first set of terms in (102) gives the real part of $\langle \delta\gamma\rangle_{t_o\varphi_o}$, and the second set of terms multiplied by i gives the imaginary part of $\langle \delta\gamma\rangle_{t_o\varphi_o}$. As is shown below, Re $(\langle \delta\gamma\rangle_{t_o\varphi_o})$ and Im $(\langle \delta\gamma\rangle_{t_o\varphi_o})$ respectively determine the gyrotron start oscillation beam power and resonant frequency detuning. Averaging over the

guiding-center angle ψ_{gc_o} for a cylindrical cavity, or over x_{gc_o} for a rectangular cavity, again leads to a reduction of the double sum over cavity eigenfunctions to a single sum. After averaging, the product $\Sigma_\Gamma \mathfrak{A}_\Gamma^{I*} \mathfrak{D}_{\Gamma s}^* \Sigma_\Lambda \mathfrak{A}_\Lambda^I \mathfrak{D}_{\Lambda s}$ is replaced by $\Sigma_\Gamma |\mathfrak{A}_\Gamma^I|^2 |\mathcal{E}_{\Gamma s}|^2$ where $|\mathcal{E}_{\Gamma s}|^2$ is either $[\mathcal{C}_{\Gamma-k}^I]^2$ (or $[J_{\Gamma-k}^I]^2$ if $r_{L_o} > r_{gc_o}$) or $[\cos(k_{y\Gamma} y_{gc_o})^2 \cos(s\lambda_\Gamma)^2 + \sin(k_{y\Gamma} y_{gc_o})^2 \sin(s\lambda_\Gamma)^2]/2$, respectively, for cylindrical and Cartesian geometries. The smooth-walled limit of (102) is obtained by taking the limit $w \to 0$ or $\theta_o \to 0$ in the dispersion relation, and by using $\Gamma = m$, $\mathfrak{A}_\Lambda^I \delta_{\Lambda\Gamma} = 1$, $\mathfrak{A}_0^{II} = 0$.

The full behavior of $\langle \delta\gamma \rangle_{t_o\varphi_o}$ is clearly given by (102). The guiding-center dependence is given by the factor $\Sigma_\Gamma \mathfrak{A}_\Gamma^{I*} \mathfrak{D}_{\Gamma s}^* \Sigma_\Lambda \mathfrak{A}_\Lambda^I \mathfrak{D}_{\Lambda s}$; the resonance behavior as a function of magnetic field about the cyclotron harmonics is given by the functions g and f; the several interactions which take place simultaneously in a gyrotron are explicitly separated. Cyclotron maser and Weibel emission resonances are given by the terms in $U_{\perp_o}^2 J_s'^2/\gamma_o U_{z_o}(\cdots)$. The terms in $2sJ_s'(\cdots)$ are due to cyclotron maser absorption. Peniotron emission and absorption resonances are represented respectively by the terms with the factors $g(\lambda^-)$, $f(\lambda^-)$, $g(\lambda^+)$, and $f(\lambda^+)$. We note that (102) for a smooth-walled cylindrical cavity is equivalant to the relation derived by Brand [23], and that the real portion of $\langle \delta\gamma \rangle_{t_o\varphi_o}$ averaged over ψ_{gc_o} is in the same form given previously by Vitello and Ko [24]. For slotted cylindrical oscillators, the real part of (102) can also be shown to equal the more complicated relation by Chu and Dialetis [11], [12].

The start oscillation beam power and the frequency detuning equation for steady-state operation for any TE_{mnl} mode can be found directly from $\langle \delta\gamma \rangle_{t_o\varphi_o}$. Taking the unperturbed beam energy to be P_b, the total net energy transferred from the beam to the cavity fields is given by $P_b \langle \delta\gamma \rangle_{t_o\varphi_o}/(\gamma_o - 1)$. Quite generally [25], the starting power can be given by

$$QP_b = -8.6 \times 10^6 \mathfrak{W}(\gamma_o - 1)/\mathrm{Re}\left(\langle \delta\gamma \rangle_{t_o\varphi_o}\right) \mathrm{kW} \tag{107}$$

and the frequency detuning due to the presence of the beam is

$$\frac{\omega - \omega_o}{\omega_o} = -\frac{1}{2Q} \frac{\mathrm{Im}\left(\langle \delta\gamma \rangle_{t_o\varphi_o}\right)}{\mathrm{Re}\left(\langle \delta\gamma \rangle_{t_o\varphi_o}\right)} \tag{108}$$

where $\omega_o = (k_\perp^2 + k_z^2)^{1/2}$ is the cold-cavity frequency. For gyrotron tubes, the quality factor Q is due mainly to diffractive losses, and with a good estimate of its value obtained from cold-cavity tests (107) provides a good estimate of the actual start oscillation power required. By constrast, the linear-theory values for the frequency detuning often differ significantly from the detuning under normal high-field operating conditions [23] and should be used with caution. Again, we stress that for $r_{L_o} > r_{gc_o}$ there must be a replacement in the above relations of $\mathcal{C}^I \to J$ and $J \to \mathcal{C}^I$.

IV. Discussion

We have extended the modeling of the linear kinetic theory for gyrotron oscillators to cavities with slotted rectangular and cylindrical coaxial cross sections. The averaged beam perturbed energy change is shown in a form, (102), which is the same in rectangular and cylindrical cavities. The cavity geometry determines only $k_\perp$ and the magnitude of each harmonic contribution to the overall RF cavity field of a particular mode. For each harmonic, the functional form of the differing interactions, such as the electron cyclotron maser and the peniotron interactions, do not vary with the cavity geometry and are the same for smooth-walled and slotted tubes. Studies of the relative strengths of the interactions for smooth-walled gyrotrons [25] can therefore be applied directly to slotted cavity devices.

We apply here our results to the slotted rectangular and cylindrical cavities discussed earlier. In the case of a cylindrical cavity, we set $R_i = 0$, average $\langle \delta\gamma \rangle_{t_o\varphi_o}$ over ψ_{gc_o}, and use an axis-encircling electron beam to allow for comparison with the results of Chu and Dialetis [11], [12]. In Fig. 3 we show the E_θ RF field profile for the TE_{311} mode for a cavity with $N = 6$ and $R_o = 1.4$. As one of the major advantages of the slotted cylindrical cavity is the reduction of the start oscillation condition with increasing R_o, we plot QP_b in Fig. 4 for both the electron cyclotron maser interaction and the peniotron interaction as a function of R_o. In the figure, L_z is increased with increasing R_o to hold $k_\perp/k_\parallel$ fixed at 10.7. The decrease in QP_b with R_o is partially due to the effects of a longer cavity, but is primarily caused by the increasing slot depth. The electron cyclotron maser emission curve for 49.9 keV is terminated at the R_o value where the Larmor radius strikes the cavity wall. Our results for the electron cyclotron maser QP_b are in agreement with Chu and Dialetis. However, we find that at low-beam energy the start oscillation condition is actually *smaller* for the peniotron interaction. Chu and Dialetis give results only for the electron cyclotron maser resonances and do not consider the peniotron resonances.

As an example of the effect of slots in a rectangular cavity gyrotron oscillator, we will consider the start oscillation condition QP_b for the cavity and beam parameters investigated by Han and Ferendeci [17] for a slotted rectangular cavity gyro-TWT. For the TE_{021} mode, which Han and Ferendeci found to give strong sixth-harmonic emission, we place the electron beam in Region I at $x_{gc_o} = L_x/2$, $y_{gc_o} = R/2$. Fig. 5 shows the E_x component of the RF field. The strong fringe field observed in this figure couples very strongly with high-harmonic emission. This coupling will be significant at high harmonics since with rising harmonic number s the growth of the Larmor ra-

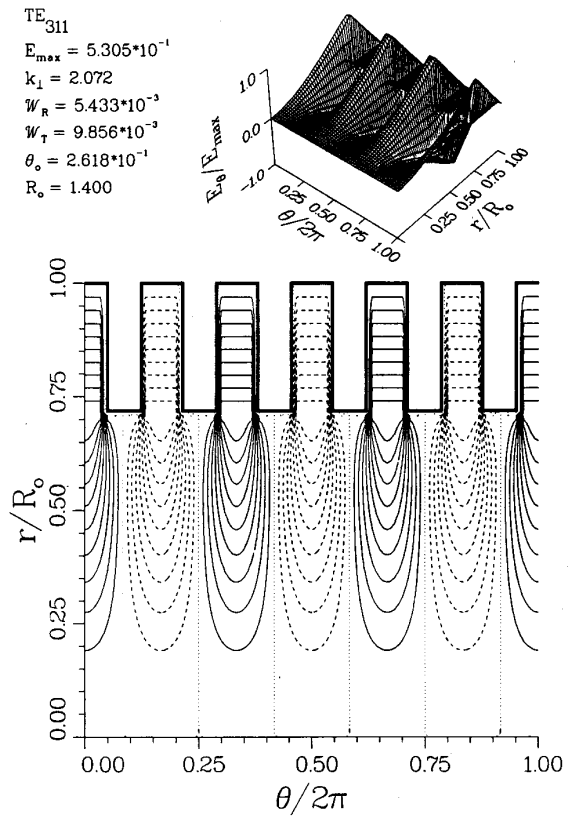

Fig. 3. E_θ RF field for a ridged cylindrical cavity with $R_o = 1.4$, $\theta_o = \pi/2N$, $N = 6$.

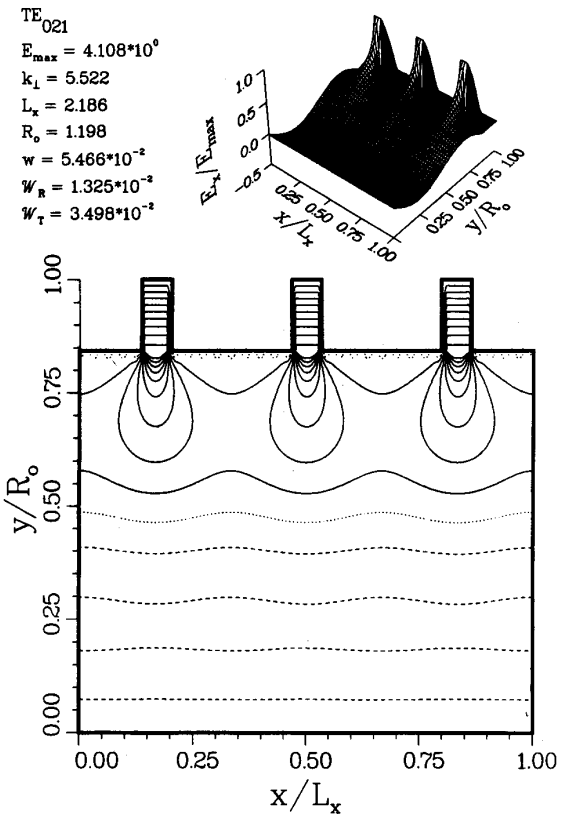

Fig. 5. E_x RF field for a ridged rectangular cavity with $L_x = 2.186$, $R_o = 1.198$, $w = 0.05466$, and $N = 3$.

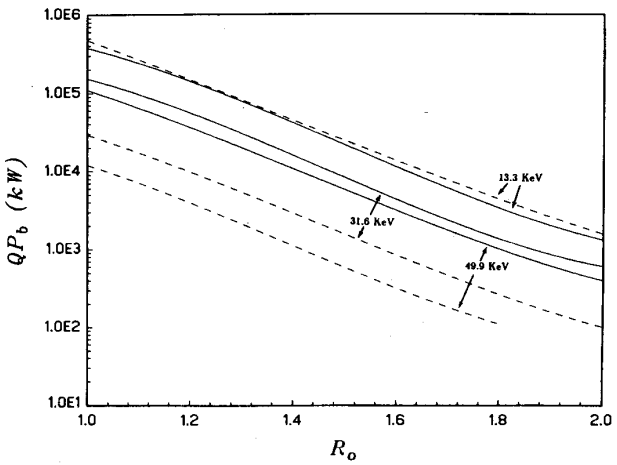

Fig. 4. Variation of the start oscillation condition for the third-harmonic electron cyclotron maser interaction (dashed curves) and second-harmonic peniotron interaction (solid curves) as a function of R_o for the TE_{311} mode. The beam axial velocity is $\beta_{z_o} = 0.1$.

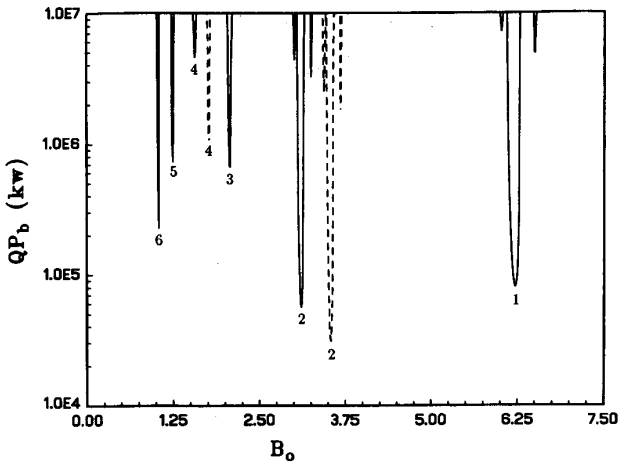

Fig. 6. TE_{021} mode start oscillation condition for the rectangular cavity for the electron beam with 72 keV, and $\beta z_o = 0.28$. The solid curve gives QP_b for the ridged cavity, while the dashed curve gives QP_b for the smooth-walled cavity.

dius, $r_{L_o} \simeq s\beta_{\perp o}/\omega$, allows the beam to increasingly penetrate the fringe fields. In Fig. 6 we show QP_b for the slotted rectangular cavity as a function of magnetic field for multiple harmonic emission. Harmonics greater than the sixth are not shown, as the beam Larmor radius would be greater than one-half the cavity width R. For comparison, QP_b for a smooth-walled rectangular cavity is also shown. For our beam position, the smooth-walled cavity only shows emission at the even harmonics. For the slotted cavity, harmonics for $s = 1$–3 are dominated by the

electron cyclotron maser instability. The fourth harmonic is due primarily to the peniotron instability. For harmonics greater than fourth, both the electron cyclotron maser and peniotron instabilities strongly contribute. It is evident that the addition of slots not only enormously enhances the very high harmonics ($s > 4$) interaction and hence greatly lowers QP_b, but this enhancement *increases* with increasing harmonic number. This descrease in QP_b with harmonic number is also implicit in the ridged gyro-TWT modeling of Han and Ferendeci. For the smooth-walled rectangular, smooth-walled cylindrical, or even ridged cylindrical cavities with axis-encircling beam previously studied in the literature, the standard behavior with increasing harmonic number is a growth in the start oscillation beam power. The high-harmonic interaction observed here for the ridged rectangular cavity shows a great potential for the practical development of a high-frequency low-magnetic-field gyrotron oscillator.

In conclusion, we find that for complex cross-gyrotron cavities the start oscillation condition can be written in a form that separates the geometric factors from the physical interaction terms. An analysis of slotted cavities using this formalism shows that slots can be used to enhance enormously the high-harmonic RF field and beam interaction for both rectangular and cylindrical cavities and also for both the fundamental electron cyclotron maser and the peniotron interactions.

REFERENCES

[1] J. M. Baird, "Survey of fast wave tube developments," in *Tech. Dig. Int. Electron Devices Meeting*, 1979, pp. 156-163.

[2] R. S. Symons and H. R. Jory, "Cyclotron resonance devices," in *Advances in Electronics & Electron Physics*, vol. 55, L. Marton and C. Marton, Eds. New York: Academic, 1981, pp. 1-75.

[3] V. L. Granatstein, M. Read, and L. R. Barnett, "Measured performance of gyrotron oscillators and amplifiers," *Int. J. Infrared Millimeter Waves*, vol. 5, pp. 267-304, 1984.

[4] D. B. McDermott, N. C. Luhmann, Jr., and D. S. Furuno, "Operation of a high-harmonic gyrotron," in *Proc. 8th Int. Conf. Infrared Millimeter Waves*, TH4.1, 1983.

[5] D. B. McDermott and N. C. Luhmann, Jr., "Operation of a compact mm-wave high-harmonic gyrotron," *Proc. SPIE*, vol. 423, pp. 58-63, 1983.

[6] W. W. Destler, R. L. Weiler, and C. D. Striffler, "High power microwave generation from a rotating e-layer in a magnetron-type waveguide," *Appl. Phys. Lett.*, vol. 38, pp. 570-572, 1981.

[7] Y. Y. Lau and L. R. Barnett, "Theory of a low harmonic field gyrotron (gyromagnetron)," *Int. J. Infrared Millimeter Waves*, vol. 3, pp. 619-744, 1982.

[8] P. S. Rha, L. R. Barnett, J. M. Baird, and R. W. Grow, in *Proc. Int. Electron Device Meeting*, 1985, pp. 525-538.

[9] R. W. Grow and U. A. Shrivastava, "Impedance calculations for traveling wave gyrotrons operating at harmonics of the cyclotron frequency in magnetron-type circuits operating at the PI mode," in *Proc. Int. Electron Devices Meeting.*, 1982, pp. 384-387.

[10] H. S. Uhm, C. M. Kim, and W. Namkung, "Theory of cusptron microwave tubes," *Phys. Fluids*, vol. 27, pp. 488-498, 1984.

[11] K. R. Chu and D. Dialetis, "Theory of harmonic gyrotron oscillator with slotted resonant structure," *Int. J. Infrared Millimeter Waves*, vol. 5, pp. 37-56, 1984.

[12] K. R. Chu and D. Dialetis, "Kinetic theory of harmonic gyrotron oscillator with slotted resonant structure," *Infrared Millimeter Waves*, vol. 13, pp. 45-74, 1985.

[13] J. Y. Choe and W. Namkung, "Experimental results of cusptron microwave tube study," *IEEE Trans. Nuclear Sci.*, vol. NS-32, pp. 2882-2884, 1985.

[14] U. A. Shrivastava, R. W. Grow, P. S. Rha, J. M. Baird, and L. R. Barnett, "Threshold power transfer for the gyrotron and peniotron oscillators operating at the harmonic cyclotron frequencies using coaxial electron beam-circuit configurations," *Int. J. Electron.*, vol. 61, pp. 33-59, 1986.

[15] P. Vitello, in *Proc. 11th Int. Conf. Infrared Millimeter Waves* (Tirrenia, Pisa, Italy), 1986, pp. 46-48.

[16] A. M. Ferendeci and C. C. Han, "Theory of high-harmonic rectangular gyrotron for TE_{mn} modes," *IEEE Trans. Electron Devices*, vol. ED-31, pp. 1212-1218, 1984.

[17] C. C. Han and A. M. Ferendeci, "Nonlinear analysis of a high-harmonic rectangular gyrotron," *Int. J. Electron.*, vol. 57, pp. 1055-1063, 1984.

[18] A. M. Ferendeci and C. C. Han, "Linear analysis on an axially grooved rectangular gyrotron for harmonic operation," *Int. J. Infrared Millimeter Waves*, vol. 6, pp. 1267-1282, 1985.

[19] Q. F. Li and J. L. Hirshfield, "Gyrotron traveling wave amplifier with out-ridged waveguide," *Int. J. Infrared Millimeter Waves*, vol. 7, pp. 71-98, 1986.

[20] J. D. Jackson, *Classical Electrodynamics*. New York: Wiley, 1962.

[21] G. B. Collins, *Microwave Magnetrons*. New York: McGraw-Hill, 1948.

[22] M. Abramowitz and A. Stegun, *Handbook of Mathematical Functions*. New York: Dover, 1972.

[23] G. F. Brand, "A gyrotron frequency detuning equation," *Int. J. Infrared Millimeter Waves*, vol. 4, pp. 919-931, 1983.

[24] P. Vitello and K. Ko, "Mode competition in the gyro-peniotron oscillator," *IEEE Trans. Plasma Sci.*, vol. PS-13, pp. 454-463, 1985.

[25] P. Vitello, W. H. Miner, and A. T. Drobot, "Theory and numerical modeling of a compact, low-field, high-frequency gyrotron," *IEEE Trans. Microwave Theory Tech.*, vol. MTT-32, pp. 373-386, 1984.